System-Level EMI of an Artificial Router System With Multiple Radiators: Prediction and Validation

Wei Zhang, *Student Member, IEEE*, Javad Soleiman Meiguni, *Senior Member, IEEE*, Kaustav Ghosh, Abhishek Patnaik, *Student Member, IEEE*, Morten Sørensen, *Senior Member, IEEE*, Ahmad Hosseinbeig, *Member, IEEE*, David Pommerenke, Jacques Rollin, Jing Li, Qian Liu, *Member, IEEE*, Philippe Sochoux, and DongHyun Kim, *Member, IEEE*

***Abstract*—In a multimodule system, an increase in the number of radiating optical modules will increase the electromagnetic emissions. This article investigates the scaled tendency of the emissions in a router system loaded with hundreds of optical modules. An artificial router mimicking the real system was built to investigate this tendency. A patch antenna array mimics the radiation of the optical modules. It can be excited in in-phase and random-phase configurations. The measurement data verifies the theoretical analysis and the prediction from a statistical method without performing hundreds of different experiments on a real router. Assuming that all radiators are radiating at the same frequency and have similar radiation pattern with random phases, the average of the maximal directivity of the system will saturate if the number of radiators (N) is larger than 14. Furthermore, the average of the maximal electric field radiated will increase following a 10 $\log_{10}$ N (dB) tendency.**

***Index Terms*—Artificial system, averaged maximal directivity ($<D_{\max}>$), averaged maximal electric field ($<E_{\max}>$), electromagnetic interference (EMI), maximal directivity ($D_{\max}$), maximal electric field ($E_{\max}$), optical modules, router system, scaling, total radiated power (TRP).**

I. Introduction

IN A BACKBONE internet router, the optical modules are the dominating radiating sources [1]. Standards such as CISPR 32 [2] and FCC part 15 [3] have specified the emission limits of the electronic devices when operating. However, they do not clearly specify a detailed guideline in handling the devices that are comprised of a large number of radiators. As a result, it is difficult to always test and debug a fully populated system reaching such complexity. In such cases, the goal is to estimate the radiation of the fully populated system as well as the uncertainty of this estimation by testing a partially populated system. To achieve this, the scaling tendency needs to be known from theory/prediction, and it must be verified by experiments. As experiments on such very complex routers are difficult to perform, alternately, a radiating structure that mimics the actual router system could be created and used for hundreds of experiments to obtain statistical data.

Mechanisms that cause the radiation of the optical modules are: common mode noise caused by the unbalanced differential pairs [4], [5]; imperfect contact between the optical module and cage, and the imperfect contact between the cage and chassis [6]–[8]. Furthermore, fiber-weave-effects in the printed circuit board (PCB) can cause common mode in the driving signal [9].

With an increased number of optical modules, the system always has the potential to fail electromagnetic compatibility (EMC) regulations [10]. Early in a project phase, it is difficult to obtain sufficient hardware for a full test. Early EMC evaluations can only be done based on the characterization of the optical modules in a mock-up system or on systems that are sparsely populated. To avoid debugging in a late project phase, it is helpful to know the scaling tendency of emissions. For systems with numbers of similar emission sources, the International Telecommunication Union recommended a statistical approach to estimate the system-level radiated emissions (RE) compliance in terms of probability [11]. Based on the individual emission of each radiator, the total emission was estimated with the assumption that the radiators have a random-phase distribution. In [12], a statistical analysis method was used to estimate the maximal increase of the radiated and conducted emissions from a multiradiator system. However, no specified tendency of the $E_{\max}$ with the number of radiators was derived. In [13], a model of a dipole antenna array excited by random phases was used to mimic the radiation performance of the sources. The estimation of $E_{\max}$ was calculated statistically from 1 000 000 cases. However, the emission prediction methods in [11]–[13] were not verified by measurement.

Manuscript received December 14, 2019; revised May 1, 2020; accepted May 30, 2020. Date of publication July 15, 2020; date of current version August 13, 2020. This work was supported by the National Science Foundation (NSF) under Grant No. IIP-1916535. This paper was presented in part at the 2019 IEEE International Symposium on EMC and SIPI, New Orleans, LA, USA, July 2019. *(Corresponding author: Wei Zhang.)*

Wei Zhang, Javad Soleiman Meiguni, Kaustav Ghosh, Abhishek Patnaik, David Pommerenke, and DongHyun Kim are with the EMC Laboratory, Missouri University of Science and Technology, Rolla, MO 65409-0001 USA (e-mail: wznkm@mst.edu; javad.meiguni@ieee.org; kgkb4@mst.edu; ap437@mst.edu; david.pommerenke@ieee.org; dkim@mst.edu).

Morten Sørensen is with the Center for Industrial Electronics, University of Southern Denmark, 6400 Sønderborg, Denmark (e-mail: soerensen@mci.sdu.dk).

Ahmad Hosseinbeig was with the EMC Laboratory, Missouri University of Science and Technology, Rolla, MO 65401, USA, and is now with the Department of EMC Design Engineering, Apple, Cupertino, CA 95014 USA (e-mail: ahosseinbeig@apple.com).

Jacques Rollin, Jing Li, Qian Liu, and Philippe Sochoux are with the Juniper Networks Co., Sunnyvale, CA 94089 USA (e-mail: jacques.rollin@juniper.net; lijing5683@gmail.com; lqpg4@mst.edu; psochoux@juniper.net).

This article has supplementary downloadable material available at https://ieeexplore.ieee.org, provided by the authors.

Color versions of one or more of the figures in this article are available online at https://ieeexplore.ieee.org.

Digital Object Identifier 10.1109/TEMC.2020.3006517

In [14], the $E_{\max}$ from an electrically large radiation source with multiple subradiators was determined by considering the relationship between total radiated power (TRP), the maximal directivity ($D_{\max}$), and the maximal electric field ($E_{\max}$). The $D_{\max}$ was derived theoretically from the electrical size of the radiator and statistically from the simulation model. However, no physical explanation was provided to explain the tendency of $E_{\max}$ with the increasing number of radiators. Reference [15] discusses the factors to be considered for predicting the emission growth with the number of radiators. However, the growth tendency was extracted without a systematic measurement approach for validation. In [16], a statistical model based on the actual radiation characteristics of the optical modules was proposed. Possible reasons for the observed discrepancies between the measured and predicted $E_{\max}$ of the actual system are discussed in [17]. The authors of [18] discussed the correlation between different RE test methods and mathematically addressed the uncertainties in the conversion between the results from different test sites. However, for achieving the goal of basing regulatory compliance on combining limited measurements with a prediction of the full system, a more comprehensive validation is needed from measurement.

The main contribution of this article lies in providing a well-controlled artificial system, which allows to vary different EMC-related parameters. This allows to validate our statistical analysis model of the tendency of radiation increase which is observed when the number of radiators increases. The advantage of the artificial system is its flexibility to operate in different controlled configurations. It allows for selection in-phase or random phase radiation of the different antennas, and they can be driven at the same frequency or slightly different frequencies.

This article expands upon the information provided by the authors in [17]. Using experimental methods, it studied the increase of system-level EMI when adding radiators, and it validates the theoretical analysis and prediction provided in [17]. This is achieved by: 1) designing an artificial with similar radiation characteristics as the actual router system; 2) analyzing measurement data on the EMI tendency with an increasing number of radiators for different phase configurations; 3) and using measurement data to validate the simulation model and analysis provided in [17].

The rest of this article is organized as follows. Section II uses the antenna array theorem and statistical simulation model to discuss the scaling tendency of the averaged maximal directivity ($<D_{\max}>$) and the averaged maximal electric field ($<E_{\max}>$) with the increasing number of radiators. Section III introduces the design of the artificial system. A comparison of the radiation characteristics between the single patch antenna and the optical module is provided. Section IV is devoted to the validation of the scaling tendency of $<E_{\max}>$ under different system configurations. Finally, Section V concludes this article.

II. Scaled EMI Tendency: Theory and Prediction

A. Theoretical Analysis of the Scaled EMI Tendency

Fig. 1 presents the router system. It was loaded with 15 line cards (LCs), each of which houses 30–36 plug-in optical modules. The unintentional radiation is mainly around 10.31 GHz. The fully loaded system contains 16 LCs with more than 400 optical modules. Therefore, it is assumed that the leakage emission from the optical modules dominates the total radiation of the whole system at 10.31 GHz.

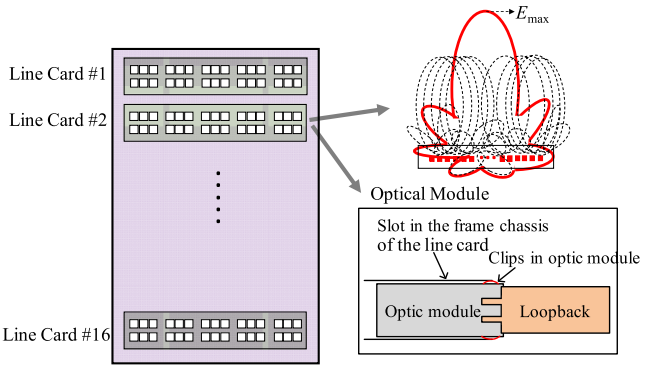

Fig. 1. Router system description.

Normally, most optical modules in the system are from the same vendor and have similar mechanical structure. It is reasonable to assume that they also have similar radiation characteristics. Other radiation sources, such as cooling vents, are well controlled. Therefore, the loaded system can be considered to be an antenna array of radiating optical modules.

As unintentional radiators, the radiation efficiency of each optical module is very low. Therefore, the mutual coupling between the optical modules can be neglected. For an array of *N*-element antennas in the location (X_n, Y_n, Z_n), the far-field strength can be expressed as [19] follows:

$$E(\theta,\varphi) = E_0(\theta,\varphi)\sum_{n=1}^{N} A_n \exp(jk\Psi_n) \tag{1}$$

where $E_0(\theta,\varphi)$ is the radiation pattern of a single element along the θ axis and φ axis; A_n describes the excitation strength; Ψ_n is the phase relationship for adjacent elements

$$\Psi_n = \Phi_n + X_n\sin(\varphi)\cos(\theta) + Y_n\sin(\varphi)\sin(\theta) + Z_n\cos(\varphi) \tag{2}$$

where Φ_n is the initial phase of each element.

Not only are the phase relationships between the optical modules within one LC important, in addition, one also needs to consider the phase relationship between the LCs.

Theoretically, if all optical modules radiate in phase, a high gain antenna radiating into the frontal direction will be formed [20]. As the number of radiators increases, the value of $D_{\max}$ will increase with 10 $\log_{10}$ *N* (dB) and the same does the TRP. Therefore, $E_{\max}$ will increase following a 20 $\log_{10}$ *N* (dB) tendency, with *N* being the number of radiators.

The system considered in this study had fixed, random-phase relationships between the optical modules within each LC, which is discussed in detail in Section III, part B. However, each LC used its own crystal (XTAL) source. Thus, frequencies between LCs differed by a few kHz. Within one LC, the radiation

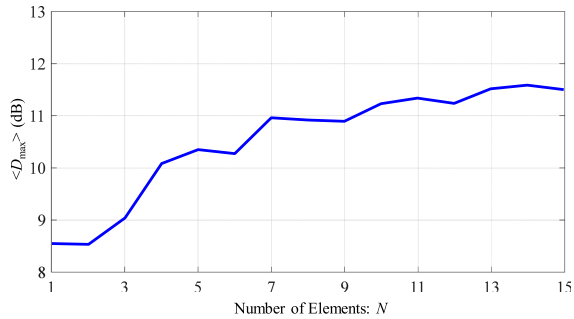

Fig. 2. $D_{\max}$ tendency with increasing number of radiators using the model provided in [16].

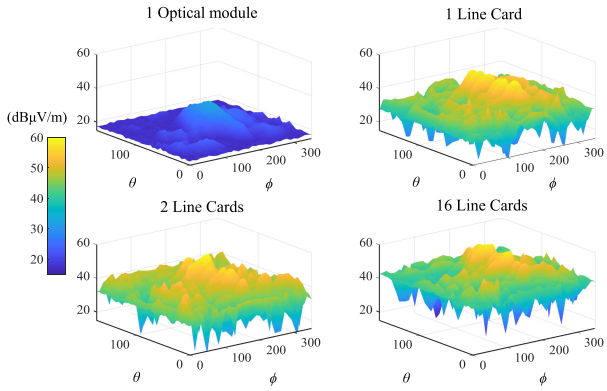

Fig. 3. E field pattern of 1 optical module, 1 LC, 2 LCs, and 16 LCs in one random-phase realization in simulation [17].

frequency between each optical module is the same. There are no time-invariant phase differences between LCs. In this case, the frequency differences are small enough to capture the total power of all the signals within one standard resolution bandwidth of the receiver during EMI testing (1 MHz).

However, if each element is fed by a random-phase signal, it is unlikely that the array forms a high-gain antenna radiating in one specific direction. If many different phase realizations are analyzed statistically and $D_{\max}$ and $E_{\max}$ is determined for each realization, in a certain angle, waves from some radiators will add constructively and waves from other radiators will add destructively. After a certain number of the radiators are added, it is very unlikely that the addition of more radiators will add constructively in one direction, and hence, the directivity ($<D_{\max}>$) saturates, which is observed in [16] and [17]. The saturation of the $<D_{\max}>$ was also observed in [18]. The value of the $<E_{\max}>$ does not follow the 20 $\log_{10} N$ (dB) tendency.

Fig. 2 shows an example of the $<D_{\max}>$ tendency for an array of radiators having the same radiation pattern and frequency as well as random-phase distribution. $<D_{\max}>$ shows a saturation phenomenon when the number of radiators is larger than 14. The value of $E_{\max}$ in the far field can be related to the TRP and $D_{\max}$ by [17]–[21]

$$E_{\max} = \frac{1}{R}\sqrt{\frac{\eta_0}{4\pi}\mathrm{TRP} \times D_{\max}} \tag{3}$$

where η_0 is the wave impedance in the free space. The total power radiated by the device under test (DUT) is TRP. The observation distance from the source is R. From (3), if $<D_{\max}>$ saturates, $<E_{\max}>$ will follow the tendency of TRP. The TRP is calculated as the spherical integral of the effective radiated power $P(\theta, \varphi)$. Numerically, it can be calculated by adding the sampled values of the power at N locations along the θ axis and M locations along the φ axis, shown as follows:

$$\mathrm{TRP} = \frac{1}{4\pi}\int_0^{2\pi}\int_0^{\pi} P(\theta,\varphi)\sin\theta \mathrm{d}\theta\mathrm{d}\varphi$$

$$\approx \frac{\pi}{2NM}\sum_{n=1}^{N}\sum_{m=1}^{M} P(\theta_n,\varphi_m)\sin\theta_n. \tag{4}$$

Therefore, for the random-phase distribution of an antenna array with similar radiating elements, the far-field $<E_{\max}>$ under many phase configurations of the elements was expected to follow a 10 $\log_{10} N$ (dB) tendency. As the TRP of the array increases linearly with the number of elements, the corresponding $<D_{\max}>$ will saturate when the number of elements is larger than 14.

B. Statistical Simulation Model

By measuring the emissions loaded with one optical module in one LC, the emission of a fully loaded system (16 LCs, each with 30 optical modules) can be predicted using the statistical simulation model proposed in [16] and [17]. The statistical model is based on the phase array antenna theorem and Monte Carlo simulation. The input of the model is the three-dimensional (3-D) radiation pattern of the single radiator, number of the radiators, the distance between each radiator, and the distance of the observation point. The output of this model is a cumulative distribution function (CDF) describing the probability P(x) that the variable takes a value less than or equal to x, i.e., P(x) $\leq x$. This function gives a reliable prediction of the averaged total electric field emission ($<E_{\max}>$) from the DUT, which helps compare of the emissions to the standard limit.

The prediction assumes that the dominant radiating sources are the optical modules. The phase distribution is discussed in Section III, subpart B and in [15] and [16]. The phase shift between each module was random but repeatable. Each LC had different phase distributions. Therefore, it is reasonable to consider a random phase distribution for the radiators in the prediction procedure for each LC. The phase distribution of the radiators forms an independent random variable with uniform distribution. This makes the phased array antenna model an orthogonal model with all the independent variables in the model are uncorrelated. Since, we ran the predictive model for thousands of iterations, we can get a CDF of $<E_{\max}>$ and make the prediction of $<E_{\max}>$ lower than a certain value with a certain probability.

All the radiators are under the following assumptions: 1) the same radiation frequency; 2) the same radiation pattern; 3) radiation observed at the far-field region. Fig. 3 shows the radiation pattern of 1 optical module, 1 LC (16 optical module), 2 LCs, and 16 LCs under a certain random-phase distribution. The

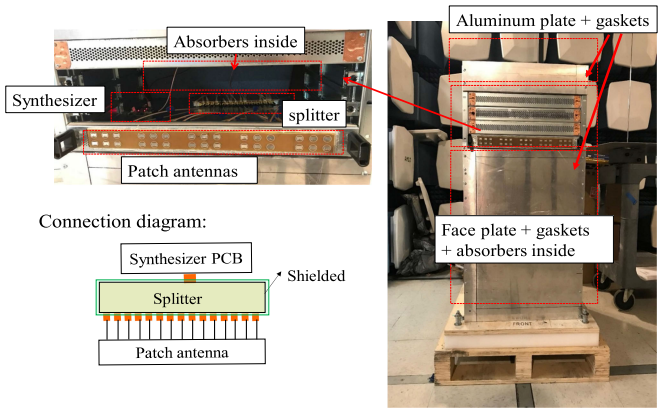

Fig. 4. Artificial system description.

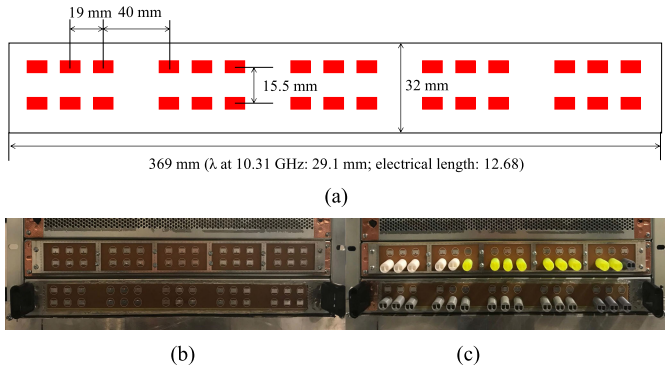

Fig. 5. Patch antenna array and the system with different source configurations. (a) Dimensions of patch antenna array. (b) Patch antenna array. (c) Patch antenna array with optical fiber cables.

total radiation energy of the subsystems is randomly distributed to the front direction due to the random-phase distribution.

When the LCs are at slightly different frequencies (several kHz), the $<E_{\max}>$ was expected to follow a tendency slower than 10 $\log_{10} N$ (dB), i.e., 8 $\log_{10} N$ (dB). The total radiation measured by the instrument is added by power intensities instead of complex fields, which is discussed in detail in [17].

III. Artificial System Design

Analyzing the emissions of an actual system for the effect of EMC relevant parameter variations such as the phasing of the radiators is difficult. These systems have no built-in function to vary such parameters. Therefore, a simplified artificial system is built to not only mimic the radiation, but also to allow the analysis via repeated measurements under different phase excitations of the radiators. Once the behavior of the artificial system is validated against simulation, the statistical method can be applied to predict the emissions of a fully loaded system.

To avoid the complexity and cost of experiments on a real router system, an artificial system was built to mimic the real router system. It provides the RF excitation and allows control of the power, pattern, and phase at each radiating element. As shown in Fig. 4, the artificial system consists of five parts: a high-frequency synthesized source, power divider, patch antenna array, varying-length cables, and the chassis. The high-frequency synthesized source is set to 10.31 GHz. The power divider splits the signal with equal amplitude and phase. Cables of varying length are connected to feed the patches. By controlling the cable lengths and the number of patches used, the radiation of the actual router is reproduced. For each realization of different phases, the cables with different lengths are randomly exchanged.

A. High-Frequency Synthesized Source

An ADF3555-based synthesizer provides −5 dBm at 10.31 GHz. Two Wilkinson power splitters (1 input and 16 outputs) feed the patches. The insertion loss was measured to be around 17 dB, which is 5 dB more than the value a lossless system would show.

B. Phase Control

For the actual router system under study, the relative phase of the radiation from each optical module was measured by near-field scanning using a measurement probe and a reference probe [15], [16]. The measured phase distribution for each optical module showed a random, stable distribution between –180° and 180°. Rebooting did not change the phase, but each LC showed a different phase distribution. To mimic this random behavior, repeated measurements used different cable lengths to feed the patches.

C. Patch Antenna Array

A patch antenna array was designed initially to mimic an LC. Similar to the arrangement of the optical modules in the LC, two rows (each having 15 patch antennas) are used. However, unlike the radiation pattern of an optical module, a single patch antenna has a wide 3 dB beam width (≈ 96°). To narrow the beam width, a dielectric rod made of 3-D printed polylactic acid (relative permittivity ≈ 3.5) material was mounted in front of the patch antenna. Fig. 5 shows the patch antenna array with and without rods. The rod bundles the beam of each patch antenna as it acts as a dielectric antenna. In the end, the single patch antenna has a dominating polarization in vertical polarization similar to a single optical module [15].

The reflection coefficient ($|S_{11}|$) of a single patch antenna with and without the rod is shown in Fig. 6. The holes on the rods are designed for the option of plugging in the fiber cables, similar to the optical modules. The resonant frequency for the designed patch antenna with rod was around 10.31 GHz. The simulation was done in CST Microwave Studio [21]. Compared with the single patch antenna without the rod, the 3 dB beam width is reduced to 56°. For the single patch antenna with/without rod, most of the energy in these two cases radiates at 10.31 GHz. Therefore, in this study, by using the patch antenna array either with or without the rod as the source does not affect the conclusion of the EMI tendency with the increasing number of radiators in this article. This will be further shown in the measurement results in Section IV.

Adding 3-D printed structures to the patches allows mimicking of the radiation pattern of other optical modules without

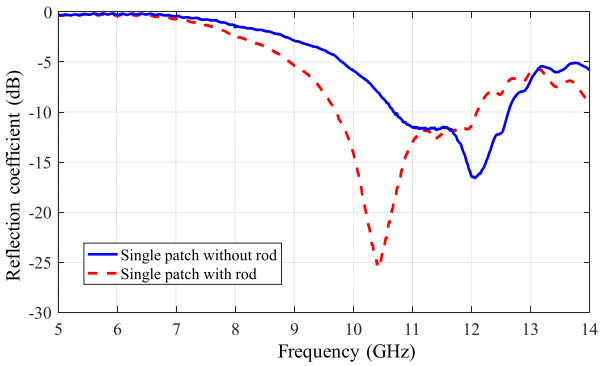

Fig. 6. Reflection coefficient of a single patch in different configurations.

TABLE I
COMPARISON OF RADIATION CHARACTERISTICS BETWEEN SINGLE OPTICAL AND PATCH ANTENNA WITH ROD

Parameters	Single optical	Patch antenna (fed with -69 dBm)
Frequency (GHz)	10.31	10.31
3 dB beam width	45°	56°
Dominating polarization [16]	Vertical polarization	Vertical polarization
Directivity (dB)	7.7	8.5
TRP from radiation pattern (dBm)	-69.2	-68.7
E_{max} measured at 2 m (dBμV/m)	37.2	38.5

having to change the PCB or feed structure. It further allows changing the radiated power of individual patch antennas by partially printing carbon loaded filaments that add loss to the dielectric extension.

D. Comparison of the Radiation Characteristics Between a Single Optical Module and Patch Antenna With Rod

The radiation pattern of a single patch antenna with rod and the single optical module was measured in an anechoic chamber at 2 m [15], [23]. The 3 dB beam width, dominating polarization, directivity, TRP and $E_{\max}$ at 2 m could all be derived from the measured radiation pattern [19].

Fig. 7 shows the comparison of the *E* field pattern between the single patch antenna with rod and the single optical module in the $\theta = 90°$ and $\varphi = 0°$ planes, vertical polarization. The radiation pattern of the patch antenna with rod matches the single optical module in the main radiation direction and polarization.

Table I compares the single optical module and the patch antenna with rod for: 3 dB beam width, dominating polarization, directivity, TRP, and $E_{\max}$ at 2 m distance. The similarity allows the use of the artificial system to mimic the real router.

IV. $E_{\max}$ SCALING VALIDATION AND DISCUSSIONS

Based on the artificial router system, the scaling tendency for TRP, $D_{\max}$, and $E_{\max}$ was measured under different configurations. The measurement was done to validate the prediction on the scaling tendency of $<D_{\max}>$ and $<E_{\max}>$ from theoretical

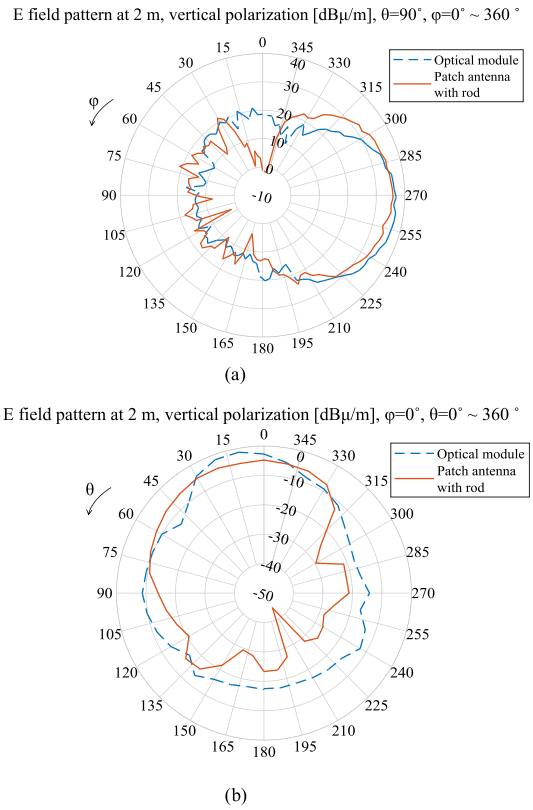

Fig. 7. Comparison of 2-D radiation pattern between patch antenna and optical module. (a) $\theta = 0°$, $\varphi = 0$ ° to 360°. (b) $\varphi = 0°$, $\theta = 0$ ° to 360°.

analysis and the statistical model based prediction given in Section II.

A. TRP Tendency Using 1–30 Elements in Random Phase

It is expected that the TRP will increases linearly as more radiators are added into the system. Therefore, TRP will follow 10 $\log_{10} N$ (dB) tendency if each radiator emits the same power. To verify the behavior of the whole system, the TRP was measured for 1–30 patch antenna excitations in a reverberation chamber tent [24]–[27]. TRP was measured by averaging the received signal 500 times while shaking the tent to stir the modes. Each patch was fed with the power of –25.5 dBm at 10.31 GHz. By exciting different numbers of patch antennas and terminating the unused outputs of the power splitter, the TRP from 1 to 30 patch antennas was measured and compared in Fig. 8. When only one antenna was excited, the received TRP was 2.7 dB larger than expectation as the radiated power of the synthesizer PCB itself was already –25 dBm. Measurement results showed that the TRP of multiple patch antennas added up linearly indicating a reliable test system.

B. Scaled $E_{\max}$ *For 1, 2, and 4 Patch Antennas With In-Phase Excitations*

For the in-phase configuration, the scaling tendency of $E_{\max}$ was analyzed with 1, 2, and 4 patch antenna elements. As the initial excitation phase of each patch is the same, the spacing between each patch antenna will determine the beamforming of

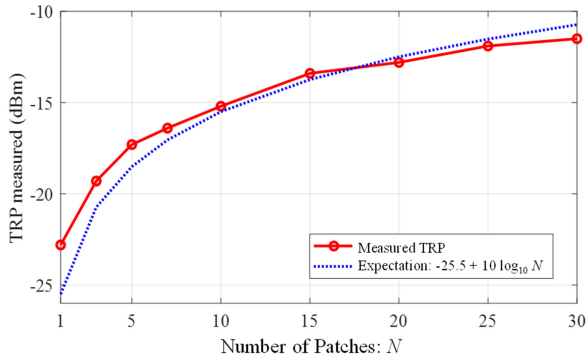

Fig. 8. Comparison between measured TRP and expectation for 1–30 patch antennas.

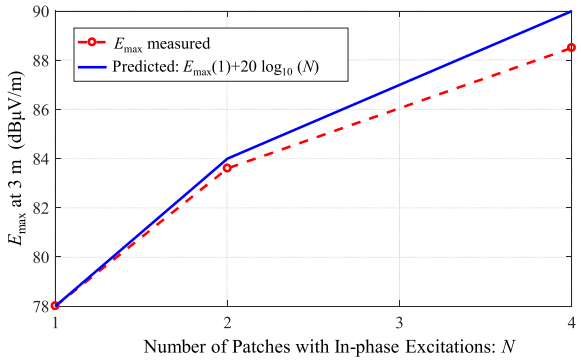

Fig. 9. $E_{\max}$ tendency with number of patches under in-phase excitations.

the antenna array. In this configuration, the comparison between the measurement and theoretical expectation provided validation for the whole radiation emission (RE) set-up with the system under test. In the RE test set-up, a horn antenna (ETS-Lindgren 3115) was mounted on the antenna tower to perform a 1.5 m height scan with a step of 0.15 m. Absorbers were put on the floor to prevent the reflection from the ground. The $E_{\max}$ radiated from the artificial system at 3 m distance was measured during RE height scan.

As the measurement configuration is only valid for an antenna array with 2 and 4 elements radiating at 10.31 GHz, the measured $E_{\max}$ at 3 m is in the far-field region considering the electric size of the array. Under in-phase configuration, $E_{\max}$ is expected to follow the 20 $\log_{10}$ N (dB) tendency with the number of radiators.

Fig. 9 shows the measured $E_{\max}$ tendency for in-phase excitation at 3 m distance at 10.31 GHz. The $E_{\max}$ of the in-phase antenna array shows a tendency close to 20 $\log_{10} N$ (dB) with the increasing number of radiators. This matches with the theoretical analysis for the in-phase antenna array. Besides, this observation offers validation on the performance of the RE test set-up with the artificial system.

C. $<E_{\max}>$ Tendency For 15, 20, 25, and 30 Elements With Random-Phase Excitations

For the random-phase configuration, the scaling tendency of $E_{\max}$ was analyzed using 15, 20, 25, and 30 patch antenna elements. In this configuration, the spacing between each patch

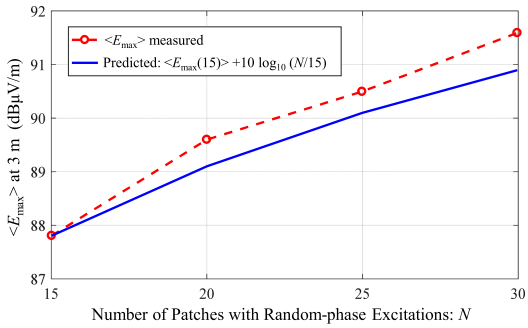

Fig. 10. $<E_{\max}>$ tendency in random phase excitations.

antenna is no longer important as the statistical term $<D_{\max}>$ and $<E_{\max}>$ are studied from thousands of different random-phase distributions for the initial excitation phase of each patch antenna. Each element was fed with the RF power of around –31 dBm with 3 dB variations. As random-phase excitations will give different emissions, statistical analysis should be based on the measured data under different random-phase cases. Randomization was achieved by switching the feed cables with different lengths from the splitter to the antennas. This was repeated six times for each number of the patch antenna elements. The value of $<E_{\max}>$ gives the average of the six tests statistically.

By comparing the tendency of EMI with an increasing number of radiators in simulation and measurement on the artificial system, validation is made on the estimation from statistical analysis. Two cases were studied in the random-phase configuration in terms of different sources: 1) Patch antenna array, 2) Patch antenna array with dielectric rods.

For the patch antenna array as the radiation source, the comparison of the measured and theoretically expected $<E_{\max}>$ tendency, relative to the number of radiators, is shown in Fig. 10. As is discussed in Section II, when the phase distribution of the radiators is random, statistically the $<E_{\max}>$ will only follow the tendency of TRP as the directivity saturates when the number of the radiators increases larger than 14. The tendency of the measured $<E_{\max}>$ with the increasing number of radiators is close to 10 $\log_{10} N$ (dB) tendency, which validates the theoretical analysis. The predicted $E_{\max}$ range for 15 and 30 patch antennas under random-phase configuration with different probabilities is shown in Fig. 11. For the artificial system with patch antenna array in random-phase distributions, the measured $<E_{\max}>$ under different phase randomizations fell into the 40% to 90% probability range. With a large quantity of samples, it is possible for the measured $<E_{\max}>$ to reach the minimum and maximum limit, which the prediction shows.

Similarly, the measured and predicted $<E_{\max}>$ of the artificial system for 16 to 30 patch antennas with dielectric rods in random-phase excitation is shown in Figs. 12 and 13. For the excitation of 15 patch antennas with rods, the measured $<E_{\max}>$ under different phase randomizations fell into the 20% to 90% probability range. For the excitation of 30 patch antennas with dielectric rods under different random-phase distributions, the measured $<E_{\max}>$ under different phase randomizations fell into the 10% to 60% probability range.

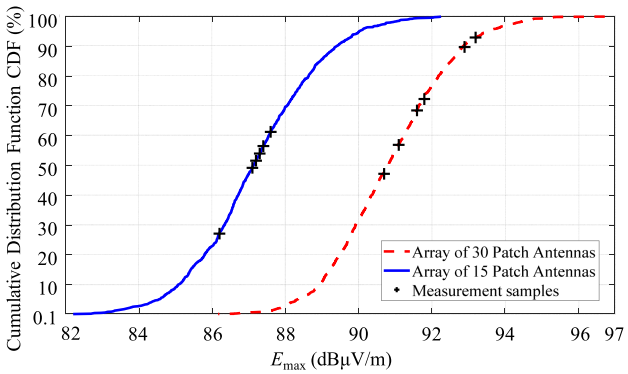

Fig. 11. Measurement samples (black cross) and prediction (blue and red).

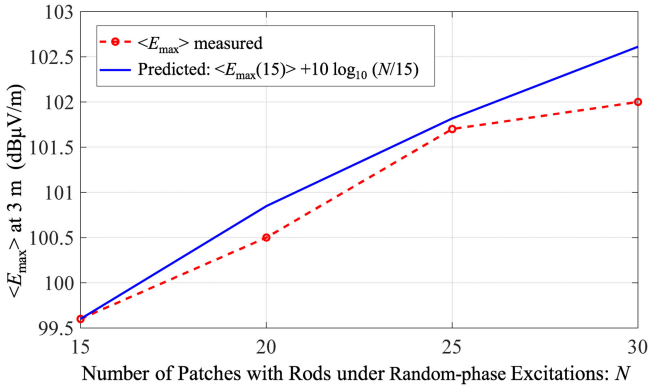

Fig. 12. $<E_{\max}>$ tendency in random phase excitations.

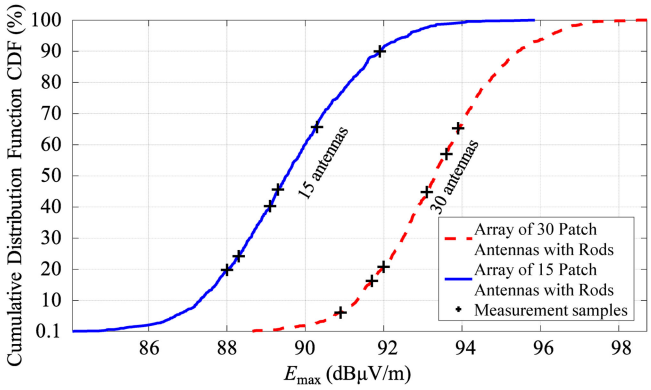

Fig. 13. Measurement results and prediction.

In the two cases investigated with random-phase distributions, the $<E_{\max}>$ with an increasing number of radiators all follows the tendency close to 10 $\log_{10} N$ (dB). This validates the prediction from the simulation and theoretical analysis.

From the EMC point of view, the difference between simulation and measurement is within 2 dB. The possible reasons for the difference between measurement and simulation are: 1) the number of samples that we measure for random phase distribution may not be enough to get statistical $<E_{\max}>$, for example, $<E_{\max}>$ is obtained based on the measurement for six times random phase distribution; 2) possibilities to miss the

TABLE II
TRP FOR 15–30 PATCH ANTENNAS

Number of patches	TRP rods (dBm)	TRP rods + fibers (dBm)
15	-20.7	-21.0
20	-18.8	-19.0
25	-17.9	-18.0
30	-17.5	-17.5

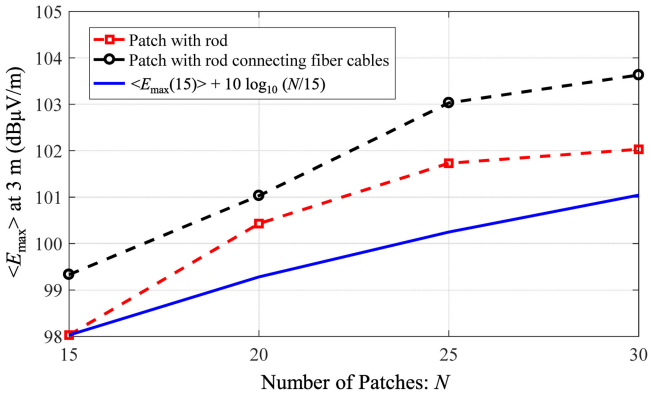

Fig. 14. $<E_{\max}>$ tendency for 15–30 patch antennas with rod/rod + fiber cables.

$E_{\max}$ peak in the RE measurement, such as receiving antenna height step and turntable rotation angle during the RE scan, which is discussed in [17]. To reduce the error, more number of samples measured in the random-phase distribution and finer scan step in RE measurement are suggested.

D. *Effect of Optical Fiber Cables on the Radiation*

The rods in front of the patch antennas mimic the fiber connector (normally made from plastic material but may also contain a ceramic section and a metal ring). The structure can have wave guiding and beam forming effects, it may also introduce losses or scatter the signal to the sides.

In the real system, many optical fiber cables are in the path of the radiation. The loss of the optical fiber cables was investigated by measuring TRP. The scattering was measured using $<E_{\max}>$ with/without fiber cables. Comparing columns 2 and 3 of the measured TRP in Table II, it shows that the optical fiber cables do not absorb at 10.31 GHz.

The scattering effect of the optical fiber cables was also investigated by observing the $<E_{\max}>$. For 15 and 30 antennas excited in random phases, $E_{\max}$ was measured with/without fiber cables for six times with the phase randomization. Fig. 14 shows the $<E_{\max}>$ tendency with the number of radiators with/without fiber cables. They are all close to the 10 $\log_{10} N$ (dB) tendency. Therefore, no significant effect on the lossy or scattering of the fiber cables was observed.

E. *Discussion of* $E_{\max}$ *and TRP Correlation With Directivity*

When there are large numbers of radiators in the system with random-phase distribution, the $<E_{\max}>$ and TRP can be obtained from measurement. Thus, the $<D_{\max}>$ can be obtained from (3). According to the statistical model proposed in [16] and

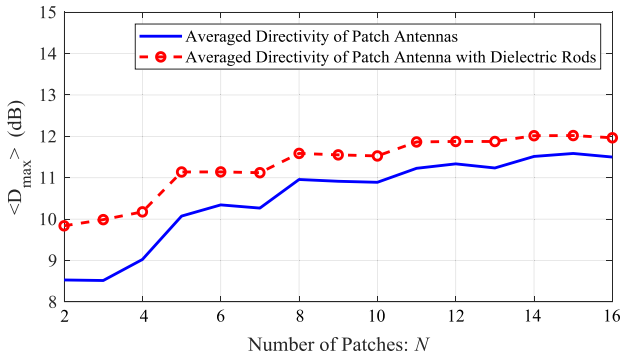

Fig. 15. Saturation of directivity as number of radiators increases.

TABLE III
TRP, DIRECTIVITY, AND $E_{\max}$ CORRELATION

Parameters to be compared	30 Patch antennas	30 Patch antennas with rods
TRP measured	-16.4 dBm	-17.5 dBm
$<E_{\max}>$ measured at 3 m	91.6 dBμV/m	91.78 dBμV/m
$<D_{\max}>$ predicted by the statistical model	12 dB	12.5 dB
$D_{\max}$ calculated from (3)	12.9 dB	13.9 dB

[17], a prediction on $<D_{\max}>$ of the artificial system based on the radiation characteristics of a single radiator can be obtained statistically from random-phase realizations for 1000 times. By comparing the $<D_{\max}>$ obtained from (1) and the statistical simulation model, the validation of (1) and the saturation of $<D_{\max}>$ in the random phase configuration can be proved.

From the statistical model, for a patch antenna array with 30 patch antennas fed by 30 random-phase excitations at the same frequency, the $<D_{\max}>$ was saturated to 12 dB when the number of radiators is larger than 14. Similarly, for the antenna array with 30 patch antennas with rods, the $<D_{\max}>$ was saturated to 12.5 dB. These are shown in Fig. 15. In both cases, $<D_{\max}>$ was calculated using (1) based on the measured TRP and $<E_{\max}>$. Table III shows the measured TRP, measured $<E_{\max}>$, $<D_{\max}>$ obtained from statistical simulation model, and the $<D_{\max}>$ calculated from (1) with the measured TRP and $<E_{\max}>$.

The error between the $<D_{\max}>$ from (1) and the statistical model is within 1.5 dB, validating the simulated $<D_{\max}>$ by measurement. These significant results confirmed that for the random-phase excitations in the system, the $<D_{\max}>$ saturated when the number of radiators was larger than 14, and the $<E_{\max}>$ trended to follow the $10\log_{10} N$ (dB) formula.

V. CONCLUSION

In this article, the EMI tendency of a multiradiator system with an increasing number of radiators is discussed with theoretical and a statistical analysis model. A scalable artificial system was designed to mimic the actual RE from the real router for this study. By analyzing the emission behaviors of the single optical module in the actual router, the artificial system was designed to be able to generate similar element radiation performances based on a patch antenna array. Furthermore, the artificial system provided a strong evidence of the $E_{\max}$ tendency with an increasing number of radiators under different controlled configurations, i.e., in-phase/random-phase excitations. When all the radiators are in phase, the system shows a $20\log_{10} N$ (dB) tendency in $E_{\max}$. When all the radiators are in random phase and N is larger than 14, the system showed a $10\log_{10} N$ (dB) tendency in $<E_{\max}>$, following the $10\log_{10} N$ (dB) tendency in TRP as the $<D_{\max}>$ is proved to saturate. As the whole idea is based on antenna array theory, it can be applied to both single-mode and multimode optical transmission if the system can be assumed to act as an antenna array. Based on the study, in this article, the ways to reduce the emission of a router system are by using optical modules with lower radiation, controlling the phase of the channels such that the radiation is distributed in as many directions as possible, adding EMI doors with absorbers in front of the system, and spreading the frequency of each LC over more than 1 MHz to create a spread spectrum. Furthermore, the artificial system can be improved to provide evidence of the predicted $<E_{\max}>$ tendency from a router system loaded with LCs operating at different frequencies (kHz range).

REFERENCES

[1] J. Li *et al.*, "EMI coupling paths in silicon optical sub-assembly package," in *Proc. IEEE Int. Symp. Electromagn. Compat.*, 2016, pp. 890–895.
[2] Electromagnetic Compatibility of Multimedia Equipment - Emission Requirements, IEC CISPR 32, ed. 2.0, 2015.
[3] Radio Frequency Devices, Title 47 – Telecommunication, FCC part 15, 2008.
[4] T. Watanabe, O. Wada, T. Miyashita, and R. Koga, "Common-mode current generation caused by difference of unbalance of transmission lines on a printed circuit board with narrow ground pattern," *IEICE Trans. Commun.*, vol. E83-B, no. 3, pp. 593–599, Mar. 2000.
[5] H. C. Chen, S. Connor, T. L.Wu, and B. Archambeault, "The effect of various skew compensation strategies on mode conversion and radiation from high-speed connectors," in *Proc. IEEE Int. Symp. Electromagn. Compat.*, 2013, pp. 328–332.
[6] L. Zhang *et al.*, "EMI coupling paths and mitigation in optical transceiver modules," *IEEE Trans. Electromagn. Compat.*, vol. 59, no. 6, pp. 1848–1855, Dec. 2017.
[7] J. Li, S. Toor, A. Bhobe, J. L. Drewniak, and J. Fan, "Radiation physics and EMI coupling path determination for optical links," in *Proc. 2014 IEEE Int. Symp. Electromagn. Compat.*, 2014, pp. 576–581.
[8] J. Li *et al.*, "EMI coupling paths and mitigation in a board-to-board connector," *IEEE Trans. Electromagn. Compat.*, vol. 57, no. 4, pp. 771–779, Aug. 2015.
[9] L. Simonovich, *Practical Fiber Weave Effect Modeling*. Stittsville, ON, Canada: Lamsim Enterprises, White Paper, 2011. [Online]. Available: http://lamsimenterprises.com/Practical_Fiber_Weave_Modeling_Iss3_Mar2_12.pdf
[10] H. Oomori, M. Shiozaki, and H. Kurashima, "Development of a practical electro-magnetic interference (EMI) simulation in high speed optical transceivers," in *Proc. 59th Electron. Components Technol. Conf.*, 2009, pp. 1908–1913.
[11] System Level Radiated Emissions Compliance Using Mathematical Modeling. ITU-T Recommendation K.62, 2004.
[12] Q. Yu and Z. Zhang, "EMI sub-system emission limits based on statistic analysis," in *Proc. IEEE Int. Symp. Electromagn. Compat.*, 2007, pp. 1–6.
[13] D. Kawase, H. Oomori, M. Shiozaki, and H. Kurashima, "EMI suppression of 10 Gbit/s optical transceiver by using EBG structure," in *Proc. IEEE Int. Symp. Electromagn. Compat.*, 2011, pp. 33–38.
[14] P. F. Wilson, D. A. Hill and C. L. Holloway, "On determining the maximum emissions from electrically large sources," *IEEE Trans. Electromagn. Compat.*, vol. 44, no. 1, pp. 79–86, Feb. 2002.
[15] K. Ghosh *et al.*, "Growth of radiated emission in multi-modular systems," *IEEE Trans. Electromagn. Compat.*, vol. 62, no. 2, pp. 612–616, Apr. 2020.

[16] J. Meiguni *et al.*, "EMI prediction of multiple radiators," *IEEE Trans. Electromagn. Compat.*, vol. 62, no. 2, pp. 415–424, Apr. 2020.
[17] J. Meiguni *et al.*, "System level EMC for multiple EMI sources," in *Proc. IEEE Int. Symp. Electromagn. Compat.*, 2019, pp. 493–498.
[18] H. G. Krauthauser, "Statistical analysis of the correlation of emission limits for established and alternative test sites," *IEEE Trans. Electromagn. Compat.*, vol. 53, no. 4, pp. 863–875, Nov. 2011.
[19] C. Balanis, "Arrays: Linear, planar, and circular," in *Antenna Theory Analysis and Design*. 2nd ed. New York, NY, USA: Wiley, 1997, pp. 283–371.
[20] B. Menssen, H. Brech, and H. Garbe, "On determining the directivity of electrically large, unintentional electromagnetic radiators — Assessment of a real electronic equipment," in *Proc. IEEE Int. Symp. Electromagn. Compat.*, 2016, pp. 520–525.
[21] P. Wilson, "On correlating TEM cell and OATS emission measurements," *IEEE Trans. Electromagn. Compat.*, vol. 37, no. 1, pp. 1–16, Feb. 1995.
[22] CST Computer Simulation Technology. 2017, CST MICROWAVE STUDIO 2017. [Online]. Available: https://www.cst.com/2017.
[23] Testing and measurement techniques – Radiated emissions and immunity measurements in fully anechoic rooms (FARs), IEC 61000-4-22:2010-10, Norm, 2010.
[24] P. Corona, J. Ladbury, and G. Latmiral, "Reverberation-chamber research-then and now: A review of early work and comparison with current understanding," *IEEE Trans. Electromagn. Compat.*, vol. 44, no. 1, pp. 87–94, Feb. 2002.
[25] C. L. Holloway, P. F. Wilson, G. Koepke, and M. Candidi, "Total radiated power limits for emission measurements in a reverberation chamber," in *Proc. IEEE Int. Symp. Electromagn. Compat.*, 2003, pp. 838–843, vol. 2.
[26] F. B. J. Leferink, "Using reverberation chambers for EM measurements," in *Proc. Soft COM 18th Int. Conf. Softw., Telecommu. Comput. Netw.*, 2010, pp. 1–5.
[27] R. Vogt-Ardatjew, S. van de Beek, and F. Leferink, "Experimental extreme field strength investigation in reverberant enclosures," in *Proc. Int. Symp. Electromagn. Compat.*, 2014, pp. 332–336.

Wei Zhang (Student Member, IEEE) received the B.S. degree in electronic information engineering from Central South University, Changsha, China in 2014 and the M.S. degree in electronic science and technology from Beihang University, Beijing, China in 2017. She is currently working toward the Ph.D. degree in EMC laboratory with the Missouri University of Science and Technology, Rolla, MO, USA.

Her current research interests are measurement and analysis in system EMI, RFI, and ESD.

Javad Soleiman Meiguni (Senior Member, IEEE) received the M.S. and Ph.D. degrees in electrical engineering from the K. N. Toosi University of Technology, Tehran, Iran, in 2008 and 2013, respectively.

He was an Assistant Professor with Semnan University, Faculty of Electrical and Computer Engineering, Semnan, Iran, until September 2017. He was with the Electromagnetic Compatibility (EMC) Laboratory, Missouri University of Science and Technology, Rolla, MO, USA, as a Visiting Assistant Research Professor from September 2017 until August 2019. He is currently an ESD System Design Engineer with Amazon Lab126, Sunnyvale, CA, USA. His current research interests include system-level ESD design, EMC, computational electromagnetics, and antenna.

Kaustav Ghosh received the B.E. degree in electronics and telecommunication engineering from Nagpur University, Maharashtra, India in 2012 And the master's degree in electrical engineering from Missouri University of Science, Rolla, MO, USA in 2018.

Since March 2016, he has been a Graduate Research Assistant with the EMC lab, Missouri University of Science. He is currently working as an EMC Design Engineer with Juniper Networks. His current research interest includes numerical and experimental study of EMI problems at system level and board level, power supply EMC, analysis of EMI emission issues and different EMI mitigation techniques.

Mr. Ghosh is also a member of the IEEE EMC society.

Abhishek Patnaik (Student Member, IEEE) received the B.E. degree from the Institute of Technical Education and Research, Bhubaneswar, India, in 2010, and the M.S. and Ph.D. degrees from the Electromagnetic Compatibility (EMC) Laboratory, Missouri University of Science and Technology, Rolla, MO, USA, in 2015 and 2018, respectively, all in electrical engineering.

He is currently an RF Desense Engineer with Apple Inc., Cupertino, CA, USA. His current research interests include on-chip electrostatic discharge design, RF circuit design, EMC testing, grounding, and shielding techniques to improve the EMC.

Morten Sørensen (Senior Member, IEEE) received the M.S. degree in physics from Aarhus University, Aarhus, Denmark, in 2005, and the Ph.D. degree in wireless communications from Aalborg University, Aalborg, Denmark, in 2018.

From 2006 to 2017, he was EMC and Antenna Specialist with Bang & Olufsen, Struer, Denmark, including three years (2011–2014) as a Researcher and Technical Project Manager with the innovation consortium, "EMC Design – First Time Right." From 2017 to 2019, he was a Visiting Assistant Research Professor with the EMC Laboratory, Missouri University of Science and Technology, Rolla, MO, USA. Since June 2019, he has been an Associate Professor with the Centre for Industrial Electronics, University of Southern Denmark, Odense, Denmark. His current research interests include near-field scanning, emission source microscopy, electrostatic discharge, and system-level radiated emission.

Ahmad Hosseinbeig (Member, IEEE) received the B.S. degree from Shahid Bahonar University, Kerman, Iran, the M.S., and Ph.D. degrees from the K. N. Toosi University of Technology, Tehran, Iran, in 2006, 2008, and 2013, respectively, all in electrical engineering.

He was an Assistant Professor with Science and Research Branch, Islamic Azad University, Tehran, Iran, until 2016. From February 2016 to November 2017, he was a Visiting Assistant Research Professor with the Electromagnetic Compatibility (EMC) Laboratory, Missouri University of Science and Technology, Rolla, MO, USA. He is currently an EMC Design Engineer with Apple Inc., Cupertino, CA, USA. His current research interests include computational electromagnetics, system-level electrostatic discharge (ESD), and numerical and measurement techniques related to ESD/EMC in electronic devices.

David Pommerenke received the Diploma and Ph.D. degree in electrical engineering from the Technical University Berlin, Germany, in 1984 and 1996 respectively.

After working at Hewlett Packard for 5 years, he joined the Electromagnetic Compatibility Laboratory at the Missouri University of S&T in 2001 and changed to CTO at ESDEMC in 2019. Since 2020, he has been a Professor with the Graz University of Technology, Graz, Austria in the EMC and RF coexistence laboratory. He has co-authored more than 200 journal papers and is inventor in 13 patents. His research interests include EMC, RF interoperability, system level ESD, electronics, numerical simulations, and EMC measurement methods and instrumentations.

Prof. Pommerenke is an Associated Editor for the TEMC.

Jacques Rollin received the bachelor's and master's of applied science degrees in electrical engineering from the University of Ottawa, Ottawa, ON in 1987 and 1994, respectively.

He is currently employed by Flex Design Centre in Ottawa Canada. He has more than 30 years of experience in the field of electromagnetic compatibility. He has extensive experience in designing for EMC compliance in a variety of products types; military, automotive, telecom, consumer, etc. He has been involved in various areas of EMC such as simulation, tools, budgeting, grounding, large systems, shielding effectiveness, EMI from integrated devices, and EMC compliance testing. He has also been active in the field of global EMC standards and regulations.

Jing Li received the Ph.D degree in electrical engineering from Electromagnetic Compatibility Laboratory, Missouri University of Science and Technology, Rolla, MO, USA, in 2010.

From 2012 to 2013, she was a Co-Op Student with the EMC Design Group, Cisco Systems, San Jose, CA, USA. From 2015 to 2016, she worked for Apple Inc., Cupertino, CA, as an EMC Design Engineer. From 2016 to 2019, she joined Juniper Networks, Sunnyvale, CA, as an EMC Design Engineer. She is currently a Package Design Engineer with Inphi Corporation, Santa Clara, CA. Her current research interests include the radiation physics of high-speed connectors and absorbing material application on cables.

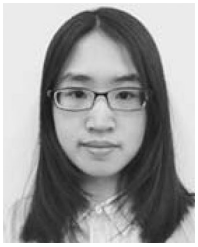

Qian Liu (Member, IEEE) received the B.S. degree from the University of Electronic Science and Technology of China, Chengdu, China, in 2013, and the M.S. degree from the Missouri University of Science and Technology, Rolla, MO, USA, in May 2016, all in electrical engineering.

From 2013 to 2016, she joined the Electromagnetic Compatibility (EMC) Laboratory, Missouri University of Science and Technology, Rolla, MO, USA. From 2016 to 2019, she was with Juniper Network, Sunnyvale, CA, USA, as an EMC Design Engineer. She is currently working with Apple Inc., Cupertino, CA, USA, as an EMC Design Engineer. Her current research interests include electrostatic discharge, absorbing material application in heatsink radiation reduction, and electromagnetic interference problem investigation on PCB.

Philippe Sochoux received the B.S. and M.S. degrees in electrical engineering from Marquette University, Milwaukee WI, USA in 1990 and 1994, respectively.

He is currently a Senior Manager for EMC Design and Product Safety with Juniper Networks. Prior to joining Juniper, he managed EMC, MDVT, safety, system ODVT and NEBS functions at Cisco Systems. He has authored or co-authored a number of papers and patents and was an invited speaker at an IEEE EMC conference.

DongHyun Kim (Member, IEEE) received the B.S., M.S. and Ph.D. degrees in electrical engineering from the Korea Advanced Institute of Science and Technology (KAIST), Daejeon, South Korea, in 2012, 2014, and 2018, respectively.

In 2018, he joined the Missouri University of Science and Technology (formerly University of Missouri-Rolla), Rolla, MO, USA, and is currently an Assistant Professor with Missouri S&T EMC Laboratory, Rolla, MO, USA. His current research interests include nanometer-scale devices, through-silicon via (TSV) technology, signal integrity (SI), power integrity (PI), temperature integrity (TI), electromagnetic compatibility (EMC) and electrostatic discharge (ESD) in 2.5D/3D IC systems.